Supporting Information for "Antarctic Circumpolar Current impacts on internal wave life cycles"

S. Waterman[1], A. Meyer[2,3], K. L. Polzin[4], A. C. Naveira Garabato[5], and K. L. Sheen[6]

[1]Department of Earth, Ocean & Atmospheric Sciences, University of British Columbia, Vancouver, Canada.
[2]Institute for Marine and Antarctic Studies, University of Tasmania, Hobart, Tasmania, Australia
[3]Australian Research Council Centre of Excellence for Climate Extremes, University of Tasmania, Hobart, Tasmania, Australia
[4]Woods Hole Oceanographic Institution, Woods Hole, Massachusetts, USA
[5]University of Southampton, National Oceanography Centre, Southampton, UK
[6]University of Exeter, Penryn, UK

Contents

S1 Identification of wave features

The vertical profiles of density and horizontal velocity indicate the presence of many coherent wave-like features. These are visually identified in the profiles of the horizontal velocity anomaly and the neutral surface height anomaly, constructed by subtracting the observed profiles of horizontal velocity and neutral density from a smoothed variant of the measured profiles. The wave-like features occur as isolated signals with consistent amplitude and vertical wavelength over multiple wavelengths (for an example, see Figure S1). In this study, we systematically examine the SOFine CTD and LADCP pro-

Corresponding author: Stephanie Waterman, swaterman@eoas.ubc.ca

files for such features. We positively identify a so-called coherent wave-like feature if all of the following criteria are satisfied:

1. a coherent wave-like feature exhibits concurrent signals with a similar vertical wavelength in both the velocity anomaly and neutral surface height anomaly profiles;
2. the wave-like feature has a consistent or consistently varying wave amplitude and vertical wavelength for at least 1.5 vertical wavelengths;
3. a corresponding peak at a consistent vertical wavenumber is detected in all of the kinetic energy, potential energy and one component of the rotary motion spectra (the latter requires the feature to have a distinct polarization);
4. a matching peak in the spectral coherence between the relevant polarized component of the horizontal velocity and the buoyancy perturbation is observed.

As described in Section 3.1, the definition of these criteria results in the positive identification of 21 coherent wave-like features in the 59 vertical profiles of CTD and LADCP measurements.

We note that the features defined from the profile data in this manner are likely biased in at least two ways: first, toward waves with lower frequencies and large horizontal scales (as it is these waves that are visually discernible in the full-depth profiles); and second, toward waves with large enough amplitude to stand out from the background variability arising from the superposition of a range of waves and other oceanic motions. As such, our characterization should be considered as applying to a select subset of the full wave population present in the region.

S2 Characterization of wave properties

We characterize the coherent features identified by assuming that they are internal waves (as in, for example, Müller et al., 1978; Polzin, 2008; Meyer et al., 2016) and applying linear wave theory. In doing so, we assume that the waves can be described as small plane-wave perturbations about a background state of rest with a locally constant background stratification. We estimate the vertical wavenumber, m, from the peak in the total energy density spectrum (which, by the criteria defined above, is consistent with the vertical wavelength of the "wiggles" seen in vertical profiles of horizontal velocity and height anomalies, as well as the peak in the relevant component of the rotary motion spec-

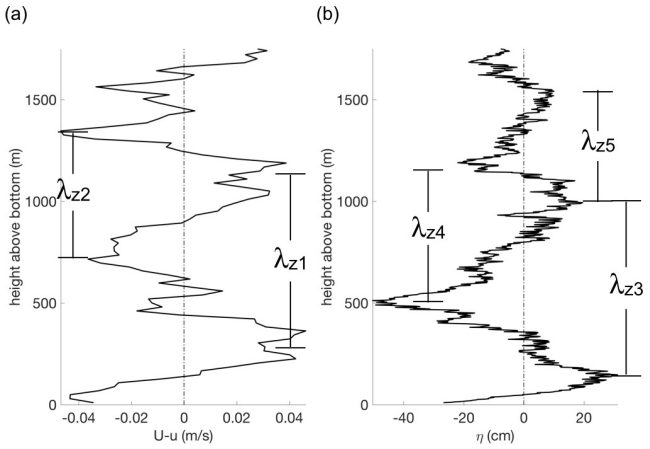

Figure S1. An example of a coherent wave-like feature seen in the vertical profiles of (a) the horizontal speed anomaly measured by the LADCP; and (b) the neutral surface height anomaly measured by the CTD. This particular example is from station 7 of the SOFine survey (see Fig. 1 of Waterman et al. (2013) for a station map). Here 2 and 3 vertical wavelengths of the feature are identified in the horizontal speed and height profiles respectively as indicated. We characterize the height of this feature as the midpoint of the vertical extent spanned by the wavelengths indicated. We characterize the vertical wavelength as the average value of all wavelengths indicated.

tra). The wave's vertical wavelength is subsequently estimated as $\lambda_z = \frac{2\pi}{m}$. The ratio of velocity variance in the clockwise- (E_{CW}) to counterclockwise- (E_{CCW}) rotating horizontal velocity components (called the rotary ratio) at this vertical scale is taken to indicate the direction of phase and energy propagation of the wave: for these Southern Hemisphere observations, a rotary ratio of less than 1 (i.e. $E_{CCW} > E_{CW}$) implies upward phase (and therefore downward energy) propagation, while a rotary ratio greater than 1 implies the opposite. Next we estimate the wave's intrinsic frequency, ω_0, from the ratio of kinetic energy, E_k, to potential energy, E_p, via $\omega_0 = f_0\sqrt{\frac{E_p(m)+E_k(m)}{E_k(m)-E_p(m)}}$. Here values of E_k and E_p are extracted from the energy spectra at the relevant vertical wavenumber m. We note that both instrumental noise, as well as 'noise' from other wave and non-wave motions is expected to bias this estimate high, we proceed with this caveat in mind. We subsequently estimate the wave's intrinsic period as $T_0 = \frac{1}{\omega_0}$. The waves horizontal wavenumber, k_H, is computed as $k_H = m\sqrt{\frac{\omega_0^2-f_0^2}{N^2-\omega_0^2}}$ (here f is the local value of the Coriolis frequency and N is the local background value of the stratification frequency, computed via the adiabatic leveling method of Bray & Fofonoff (1981) applied to the lo-

cal N profile). This assumes an approximate dispersion relation for plane-wave internal waves propagating in a low Rossby number (Ro), low Froude number (Fr), geostrophically-balanced background flow correct to order (Ro, Fr) for all hydrostatic waves (Eqn. A3 in Polzin et al., 1996). It neglects terms involving second-order derivatives of the background which are small under a WKB approximation which is implicit when the plane wave solution is invoked, and further neglects terms proportional to the relative vorticity (order Ro), the thermal wind shear (order $BuFr$, where Bu is the Burger number) and the spatial derivatives of the mean advective terms order $\frac{Bu^2 Ro}{1+Bu^2}$). This is justified by the fact that wave features are characterized by low Ro and low Fr but a Bu that is order one (see Table S1). We note that the Bu O(1) limit is highly relevant in a wave capture scenario as waves asymptotically approach the aspect ratio of the mean flow, which tends to be $Bu \approx O(1)$ for the mesoscale. Here again, we expect noise to bias our estimate of k_H high. The wave's horizontal wavelength is then estimated as $\lambda_H = \frac{2\pi}{k_H}$. We obtain an estimate of the horizontal azimuth of the wave's wave vector, ϕ, from an estimate of the phase between the relevant rotary velocity component ($u-iv$ for an upward-propagating wave, and $u+iv$ for a downward-propagating wave, where u and v are the zonal and meridional velocity components respectively) and the buoyancy perturbation at the vertical wavenumber in question. From this phase estimate, we compute the horizontal wavenumber components, k and l, as $k = \pm k_H cos(\phi)$ (for upward- and downward-propagating waves respectively) and $l = -k_H sin(\phi)$. Finally, the components of the wave's group velocity, $\vec{c_{gH}}$, are estimated from the previously computed wave properties using internal wave relations derived from the gradients of the approximate dispersion relation: $c_{gx} = k\frac{(N^2-\omega_0^2)^2}{\omega_0 m^2(N^2-f^2)}$, $c_{gy} = l\frac{(N^2-\omega_0^2)^2}{\omega_0 m^2(N^2-f^2)}$, and $c_{gz} = \frac{(\omega_0^2-f^2)(N^2-\omega_0^2)^2}{\omega_0 m(N^2-f^2)}$. Our wave characterization follows that of Meyer et al. (2016). For more details, interested readers are referred to the discussion and references therein.

S3 Characterization of the background environment

We exploit the CTD and LADCP profiles to characterize properties of the background flow and stratification environment in which the coherent wave features are observed. The background flow field is defined by smoothed variants of the LADCP velocity component profiles, specifically by applying a sliding second-order polynomial regression with an increasing vertical fit window length ranging from ∼300 m at the surface to ∼800 m at depth. The goal of the smooth fit is to eliminate variability on vertical scales

	Downward-going			Upward-going		
	mean	median	std	mean	median	std
1. WAVE PROPERTIES						
depth (for downward)/height (for upward) (m)	1321	1500	238	932	949	607
average vertical wavelength (m)	141	143	42	132	120	68
horizontal wavelength (km)	10	8	9	4	2	6
intrinsic frequency/f	1.1	1.1	0.1	2.2	1.2	3.0
intrinsic group velocity (horizontal),CgH	2.0	2.1	1.1	1.7	1.2	1.4
intrinsic group velocity (vertical) (cm/s)	-0.05	-0.04	0.04	0.2	0.1	0.3
2. BACKGROUND PROPERTIES						
horizontal speed, U (cm/s)	0.22	0.13	0.24	0.08	0.05	0.07
U/CgH	3.8	9.6	3.1	1.4	6.6	0.6
|vertical shear/N|	0.02	0.02	0.01	0.05	0.03	0.1
|strain/f|	0.1	0.1	0.07	0.08	0.06	0.01
|vorticity/f|	0.1	0.1	0.04	0.04	0.02	0.04
|Doppler shift/f|	2.3	1.0	3.7	3.3	0.8	7.6
3. TIMESCALES						
e-folding for *m* (days)	29	7	51	67	25	87
e-folding for *k* (days)	9	3	15	225	4	786
e-folding for *l* (days)	3	2	3	126	2	429
dissipation (days)	4	1	7	3	1	6
advection (days)	2	2	1	3	3	2
distance in 1 dissipation time (km)	48	22	81	33	8	62
4. RAY TRACING RESULTS						
lifetime (days)	7	6	4	12	12	12
horizontal distance (km)	188	160	129	70	70	70
5. NON-DIMENSIONAL PARAMETERS						
Rossby number, Ro	0.1	0.1	0.04	0.04	0.02	0.04
Froude number, Fr	0.02	0.02	0.01	0.05	0.03	0.1
Burger Number, Br	0.5	0.4	0.2	1.0	0.7	0.7

Table S1. Statistics summarizing the wave properties, background flow properties, timescales, ray tracing calculation results and non-dimensional parameters for all wave-like features identified. Here the Rossby number, Ro, is computed as $Ro = \frac{\zeta}{F}$ where ζ is the vertical component of the large-scale flow vorticity and f is the local Corilois frequency, the Froude number, Fr, is computed as $Fr = \frac{\frac{\partial \vec{U}}{\partial z}}{N}$ where $\vec{U}$ is the large-scale horizontal velocity and N is the background stratification, and the Burger number, Bu, is computed as $Bu = \frac{N^2 k_H^2}{f^2 m^2}$.

of a few hundred meters and less, while maintaining the large-scale structure associated with the ACC jets. Results are insensitive to the specific choice of the smoothing parameters, as long as this qualitative goal is achieved. The background stratification is defined by a smooth N profile, constructed via the adiabatic leveling method of Bray & Fofonoff (1981) applied to the local N profile with a pressure range of adiabatic leveling of 400 decibars. Again, results are qualitatively insensitive to this choice provided it remains on the order of hundreds of decibars. We use these constructed profiles to characterize the magnitude of the background flow velocity components, U and V, the magnitude of the background vertical shear, and the local background stratification and its vertical gradient in the vicinity of each observed coherent wave packet.

Our consideration of the background flow impacts on three-dimensional wave evolution is also dependent on the magnitude of the horizontal velocity gradients of the background flow. This information is unavailable from the SOFine station data: the station spacing (typically 40 km) is relatively coarse, and often provides velocity gradient information in only one horizontal direction. As such, here we rely on velocity information from satGEM (Meijers et al., 2011), a gravest empirical mode (GEM) projection of temperature and salinity fields in the Southern Ocean that, when combined with satellite altimetry, produces time-evolving temperature, salinity and velocity fields at 7-day intervals on a $1/3^o$ grid. A comparison of the observed SOFine velocity profiles to those of the satGEM at relevant times and locations produces reasonable mesoscale structure agreement, endorsing our use of the satGEM product to provide background flow and stratification information at times and places where it is unavailable in the SOFine survey observations.

S4 Timescale characterization of wave evolution

The scales characterizing the wave features, and the background flow and stratification environment through which the waves propagate and evolve, can be combined to characterize timescales that indicate the relative importance of various processes influencing wave evolution. Here we characterize the relative importance of: 1. the wave scale's modification due to the background flow's shear, strain and stratification; 2. the waves horizontal translation due to intrinsic propagation and mean flow advection; and 3. the wave's dissipation. We do this by computing the following timescales:

1. the wave-mean flow interaction timescale, $\tau_{\text{wave-mean}}$, characterizing the time it takes for the various wavenumber components of the wave to change significantly (specifically by e^{-1}) due to interaction with the background flow's shear, strain and stratification gradients. $\tau_{\text{wave-mean}}$ is computed as $\tau_{\text{wave-mean}k} = \frac{k}{-k\frac{\partial U}{\partial x} - l\frac{\partial V}{\partial x}}$, $\tau_{\text{wave-mean}l} = \frac{l}{-k\frac{\partial U}{\partial y} - l\frac{\partial V}{\partial l}}$ and $\tau_{\text{wave-mean}m} = \frac{m}{-k\frac{\partial U}{\partial z} - l\frac{\partial V}{\partial z} - \frac{\partial \sigma}{\partial z}}$ for the k, l and m components of the wavenumber, respectively. Here $\frac{\partial \sigma}{\partial z}$, the vertical gradient of the wave's intrinsic frequency, is given by $\frac{\partial \sigma}{\partial z} = N\frac{\partial N}{\partial z}\frac{k_H^2}{m^2}[\frac{N^2k_H^2 + f^2m^2}{m^2}]^{1/2}$.
2. the advection timescale, $\tau_{\text{advection}}$, characterizing the time it would take for the wave to travel away from the local environment due to both intrinsic wave propagation and advection by the background flow. $\tau_{\text{advection}}$ is computed as $\tau_{\text{advection}} = \frac{L_{Rd}}{\vec{U} + \vec{c_{gH}}}$,

where L_{Rd} is set to be a characteristic value for the local first-baroclinic Rossby radius of deformation at these latitudes, $L_{Rd} = 15$ km.

3. the dissipation timescale, τ_ϵ, characterizing the time it would take for the observed wave energy to dissipate, given the local microstructure measurement of the turbulent kinetic energy dissipation rate, ϵ (see Waterman et al. (2013) for a full description of the microstructure measurements associated with the SOFine finescale measurements discussed here). τ_ϵ is computed as $\tau_\epsilon = \frac{E(m)}{\epsilon}$, where $E(m) = E_p(m) + E_k(m)$, the total observed energy at the vertical wavenumber m in question. We note that, in general, the local measure of the dissipation rate is not that associated with the breaking of a single wave but rather the rate of energy transfer through the inertial subrange. Here we use the microstructure measure of ϵ as an appropriate order of magnitude estimate for the dissipation rate of the coherent feature energy.

An internal wave with a dissipation timescale shorter than its advection timescale will undergo local dissipation. Conversely, if the advection timescale is less than the dissipation timescale, we expect that the dissipation of the wave will be remote. The amplitude of the wave-mean flow interaction timescale relative to the dissipation timescale indicates the extent to which wave-mean flow interactions can play a role in disrupting the simple picture of a downscale energy cascade via wave-wave interactions assumed by, for example, finescale parameterizations. If $\tau_{\text{wave-mean}_m}$ is short relative to the dissipation timescale, the influence of the background flow's vertical shear will play a significant role in the evolution of the wave's vertical scale (either accelerating or opposing the downscale cascade by wave-wave interactions). If $\tau_{\text{wave-mean}_k}$ and $\tau_{\text{wave-mean}_l}$ are relatively short, the waves evolution must be considered as fundamentally 3-dimensional.

S5 Ray tracing calculations

The propagation of internal wave packets, and the evolution of their properties along a ray path for a specific background stratification and velocity field, may be mapped using ray tracing techniques (*e.g.* Lighthill, 1978; Olbers, 1981; Sheen et al., 2015). In addition to their intrinsic propagation, internal wave rays are also advected by the background horizontal current, $\vec{U}(x, y, z, t) = U(x, y, z, t) + V(x, y, z, t)$, and distorted by the local current shears, $\frac{\partial \vec{U}(x,y,z,t)}{\partial x}$, $\frac{\partial \vec{U}(x,y,z,t)}{\partial y}$ and $\frac{\partial \vec{U}(x,y,z,t)}{\partial z}$, and background stratification gradient, $\frac{\partial N(x,y,z,t)}{\partial z}$, along their ray path. Note, consistent with our approxima-

tion to the dispersion relation, we neglect the horizontal gradients of intrinsic frequency in the ray tracing equations for the evolution of the wave's wavenumber on the basis that the term arising from the thermal wind shear is small in the WKB limit. This is appropriate as the life cycle of $Bu \approx O(1)$ and larger waves is controlled by variations in the Doppler shift rather than having behavior that depends strongly upon the background relative vorticity. In this work we consider a plausible life history of the observed coherent wave packets by ray-tracing them backwards-in-time from the time and location of observation. We use the satGEM data to provide the time- and space-varying background flow and stratification fields. We use the ray tracing model to track the temporal evolution of the wave's position and characteristics using finite-differencing, with the wave position, wavenumber and frequency being updated on 10-minute time steps. We also record the temporal evolution of background flow and stratification properties along the ray path, in order to document the evolving influence of the background environment on the wave's evolution. The model is run until the wave packet intersects the seafloor or the base of the mixed layer, a period that ranged from 0.1 to 21 days.

References

Bray, N. A., & Fofonoff, N. P. (1981). Available potential energy for MODE eddies. *J. Phys. Oceanogr.*, *11*(1), 30-47.

Lighthill, J. (1978). *Waves in fluids.* Cambridge University Press.

Meijers, A. J. S., Bindoff, N. L., & Rintoul, S. R. (2011). Frontal movements and property fluxes: Contributions to heat and freshwater trends in the Southern Ocean. *J. Geophys. Res. Oceans*, *116*(C8).

Meyer, A., Polzin, K. L., Sloyan, B. M., & Phillips, H. E. (2016). Internal waves and mixing near the Kerguelen Plateau. *J. Phys. Oceanogr.*, *46*(2), 417–437.

Müller, P., Olbers, D. J., & Willebrand, J. (1978). The Iwex spectrum. *J. Geophys. Res. Oceans*, *83*(C1), 479-500.

Olbers, D. J. (1981). The propagation of internal waves in a geostrophic current. *J. Phys. Oceanogr.*, *11*(9), 1224-1233.

Polzin, K. L. (2008). Mesoscale eddy-internal wave coupling. Part I: Symmetry, wave capture, and results from the Mid-Ocean Dynamics Experiment. *J. Phys. Oceanogr.*, *38*(11), 2556-2574.

Polzin, K. L., Oakey, N. S., Toole, J. M., & Schmitt, R. W. (1996). Fine struc-

ture and microstructure characteristics across the northwest Atlantic Subtropical Front. *J. Geophys. Res. Oceans*, *101*(C6), 14111-14121.

Sheen, K. L., Brearley, J. A., Naveira Garabato, A. C., Smeed, D. A., Laurent, L. S., Meredith, M. P., ... Waterman, S. (2015). Modification of turbulent dissipation rates by a deep Southern Ocean eddy. *Geophys. Res. Lett.*, *42*(9), 3450-3457.

Waterman, S., Naveira Garabato, A. C., & Polzin, K. L. (2013). Internal waves and turbulence in the Antarctic Circumpolar Current. *J. Phys. Oceanogr.*, *43*(2), 259–282.